Article:

Dedeoglu, S. orcid.org/0000-0001-7969-011X, Konstantopoulos, G.C. and Komurcugil, H. (2022) Current-limiting virtual synchronous control and stability analysis considering DC-link dynamics under normal and faulty grid conditions. IEEE Journal of Emerging and Selected Topics in Power Electronics, 10 (2). pp. 2516-2527. ISSN 2168-6777

https://doi.org/10.1109/jestpe.2021.3103830

Current-limiting Virtual Synchronous Control and Stability Analysis Considering DC-link Dynamics Under Normal and Faulty Grid Conditions

Seyfullah Dedeoglu, *Student Member, IEEE,* George C. Konstantopoulos, *Member, IEEE,* Hasan Komurcugil, *Senior Member, IEEE*

***Abstract*—An improved nonlinear virtual synchronous control for three-phase grid-connected inverters, that can maintain a reliable operation under both normal and faulty grid conditions, i.e. balanced grid voltage sags, is proposed. The proposed controller can ensure a desired RMS current limitation at all times, provide virtual inertia and damping via the DC-link voltage and AC system frequency coupling, and realize the desired real and reactive power regulation without requiring accurate knowledge of the system parameters. Opposed to the conventional methods that use saturated PI controllers with or without anti-windup techniques to limit the reference value of the inverter current, the proposed controller includes a nonlinear bounded integrator, which limits the actual value (instead of the reference) of the inverter RMS current and leads to a fast system recovery even after significant grid voltage sags. The closed-loop stability of entire system is rigorously proven using nonlinear singular perturbation theory. Moreover, analytic conditions for the controller parameter selection to guarantee the stability of entire inverter system with the DC-link dynamics are provided. To prove the effectiveness of proposed controller and its superior performance compared to the traditional approaches, extensive Matlab/Simulink-based simulations are performed, followed by Typhoon-HIL hardware-in-the loop implementation using a TI microcontroller.**

***Index Terms*—Nonlinear droop control, RMS current limitation, virtual synchronous control, DC-link voltage control, grid faults, stability analysis, three-phase inverter.**

I. Introduction

THE notion of renewable energy (RE) based distributed generation (DG) has gained considerable popularity in the research community to modernize the conventional power grid due to the environmental and technical concerns during the last decades [1]–[3]. Although the increased number of DG units may seem harmless from the non-technical point of view, it can have a significant impact on the grid stability if not properly managed in case of system transients [4], [5]. Since the DGs, such as photovoltaic and storage units, generally require power converter interface devices, which have faster dynamics and lack of a physical inertia, for grid connection, suitable control design for these devices is essential for the reliability and stability of the power network [6]–[8].

In order to address the stability and reliability problems in modern power networks, the control algorithms of the power interface devices, which are mainly inverters in RE applications, can be designed to include the well-known droop control operation, virtual synchronous generator (VSG), and virtual oscillator control (VOC) [9], [10]. Since the traditional power systems employ high power rated synchronous generators (SGs), which can provide or extract energy to or from the power network due to their high physical inertia capability, the conventional $P-\omega$ and $Q-V$ droop method can maintain the balanced and stable operation in these systems. However, in DG applications, low power rated grid-connected inverters lack physical inertia and are sensitive against large system transients due to their switch-based structures [11], [12]. Therefore, significant efforts have been made to embed the inertia dynamics into the grid-connected inverters by imitating either the behavior or the physical characteristics of the SGs.

The behavioral characteristics of the SGs can be mimicked via the droop control approaches, such as conventional, adaptive, robust and universal droop control [13], while physical SG dynamics can be resembled via VSG methods, such as synchronverter, virtual synchronous machine, and synchronous power controller [3]. Although droop control techniques can improve the voltage and frequency control and VSG methods can provide synthetic inertia to balance the system for stability enhancement, both approaches may suffer from the overshoots, current limit violations, and stability problems if a large disturbance, such as a drastic voltage sag, occurs [10], [14]. Therefore, virtual synchronous control (ViSynC) approaches have started to gain attention, since they can merge the useful features of the droop control and VSG techniques by utilizing both the DC and AC side system dynamics [15], [16] and offer better disturbance rejection ability compared to the previously mentioned approaches in case of system faults [1], [10].

Opposed to SGs, VSGs are responsible for the reactive power regulation through their separate reactive power control (RPC) loops. Therefore, RPC can have a considerable effect on the system stability under the grid voltage sags due to the shifting of the operating point [17], [18]. Furthermore, inverter current limitation in case of abnormal system conditions is another important issue for a safe and reliable DG operation

This work is supported by EPSRC under Grants No EP/S001107/1 and EP/S031863/1, and under Grant 81359 from the Research Committee of the University of Patras via "C. CARATHEODORY" program.

S. Dedeoglu and G. C. Konstantopoulos are with the Dept. of Automatic Control and Systems Engineering, The University of Sheffield, Sheffield, S1 3JD, UK. G. C. Konstantopoulos is with the Dept. of Electrical and Computer Engineering, University of Patras, Rion, 26500, Greece. E-mails: {sdedeoglu1, g.konstantopoulos}@ sheffield.ac.uk.

Hasan Komurcugil is with the Dept. of Computer Engineering, Eastern Mediterranean University, 99628 Famagusta, Mersin 10, Turkey. E-mail: hasan.komurcugil@emu.edu.tr

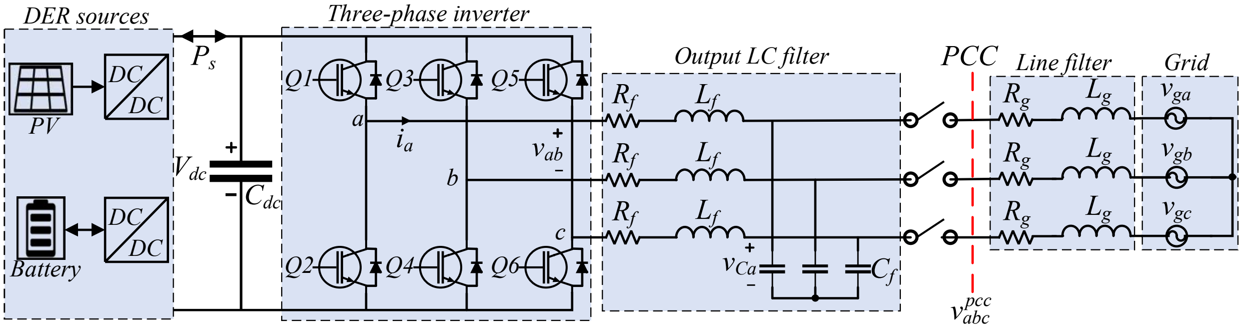

Fig. 1: DER-sourced grid-connected three-phase inverter.

and it is generally realized either via switching between different control algorithms [19] in VSGs or by using adaptive saturation methods [16], [20] in ViSynC approaches. Since the current limitation is a critical issue for a reliable power transfer operation in RE applications, considerable research effort is allocated in this topic. Virtual impedance-based methods [21]–[23] are one of the main approaches, which can be used for the purpose of current limitation for particular applications. However, those approaches use saturation units to limit the reference values of the inverter current instead of the instantaneous values, may not maintain the system stability, which is a critical issue for the converter based power generation after a substantial system fault, and examines the system stability using root-locus and bode diagram approaches around a given equilibrium point. In particular, a virtual impedance-based current-limiting algorithm is proposed for grid-forming converters in [24]. However, this method requires the threshold and maximum current values to be different; hence, it may need higher power rated circuit components for lower power applications. Moreover, the authors in [25] propose a method which has inherent current-limiting property for grid-forming inverters, but no analytic stability condition is provided to guide the prospective users for controller parameter selection, i.e., the stability is guaranteed only for a given set of system parameters and cannot be generalized for any converter. Furthermore, the authors in [26]–[28] offer current-limiting algorithms specifically for VSG converters considering various grid and load conditions. Even though the method in [26] can limit the harmonic and inrush fault current, it uses limiters in the control algorithm and requires knowledge of the grid-side line parameters in the control design process. In [27], a method that can limit transient inrush currents in synchronverters is proposed. However, this method does not include stability analysis and it may be difficult to implement since there are many algorithm changes. An MPC based fault current limiter is proposed in [28], which offers satisfactory results, but significantly increases the computational cost of the controller implementation. To this end, the previously mentioned techniques do not offer a rigorous stability analysis, cannot guarantee the desired instantaneous current limitation at all times, including large transients, cannot ensure that the system will recover to its stable operating points after a large disturbance due to unresolved integrator windup issue, and may eventually lead to system instability [29]. To address the integrator windup issue and guarantee the closed-loop system stability, the bounded integral control (BIC) concept has been proposed in [30], and applied to synchronverters [31] and three-phase rectifiers [32]. Recently, as an enhancement to the original BIC, a state-limiting PI (sl-PI) controller [33], which introduces less controller states and leads to easier implementation, has been proposed and applied to three-phase inverters [34]. However, all of these applications assume constant DC input voltage dynamics and do not examine the effect of intermittent RE sources on the system stability.

In this paper, a nonlinear control method is proposed for the three-phase VSG inverters that can both inherently limit the inverter RMS current and provide virtual inertia and damping by combining the ViSynC and droop control dynamics. The proposed approach does not employ any saturation units, does not require a power or current reference change, and does not switch between different control algorithms, e.g., from grid-forming to grid-following, in case of grid voltage sags as in [19], [20] to avoid integrator windup and eventually the system instability [29]. The structure of the proposed technique includes two parts:

1) The implementation of the droop control via sl-PI controller for accurate $Q \sim V$ control, and RMS current-limiting property,
2) The integration of the ViSynC for providing virtual inertia and damping via $V_{dc} \sim \omega$ droop dynamics.

The RMS current-limiting property holds independently from the grid and ViSynC parameters. The closed-loop stability of the whole system is rigorously proven for the first time for ViSynC inverters using singular perturbation theory for nonlinear systems [35]. In order to decrease the complexity of the system dynamics and stability analysis, the local inverter current is aligned with the d axis via controller design as in [34] contrary to the conventional approaches that align the inverter voltage with the d axis [36].

The main contributions offered in this paper are outlined in the following: 1) the DC-link dynamics are incorporated into the existing three-phase grid-connected inverter dynamics, which is also equipped with sl-PI controller, to build a more realistic nonlinear system model, provide virtual inertia and damping to the system, and achieve bidirectional power transfer opposed to [31], [32] and [34], which assume a constant DC voltage; 2) the current-limiting property is guaranteed for the instantaneous values of the current instead of the reference values without employing saturation based methods contrary to [16], [20] and [26] and without assuming small-signal stability as in virtual impedance and saturation unit based methods [21]–[23]; 3) the closed-loop stability of the

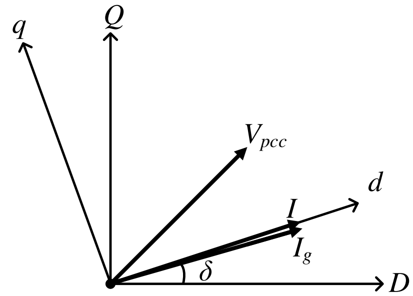

Fig. 2: Vector diagram of local (dq) and global (DQ) PCC frames.

entire system is proven using singular perturbation theory instead of root-locus or bode diagram methods as in [25]–[27] for the first time for RE-sourced three-phase inverters, according to the author's knowledge, and analytic stability and system parameter selection conditions are provided to guide the prospective users; 4) comprehensive comparison studies with the commonly-used current-limiting techniques considering the effect of well-known clamping anti-windup method are performed via Matlab/Simulink software; and 5) extensive Hardware-In-the-Loop (HIL) results using a Typhoon-HIL device and a TI F28379D launchpad are presented to prove the effectiveness of the proposed approach compared to state-of-the-art current-limiting algorithms.

II. Modeling of DER-Based Inverter System

The system under inspection is a distributed energy resource (DER)-sourced grid-connected three-phase inverter as shown in Fig. 1. The inverter is connected to a point of common coupling (PCC) through an output LC filter whose parasitic resistance, inductance, and capacitor are given as R_f, L_f, and C_f, respectively, while the grid line parasitic resistance and inductance are given as R_g and L_g. The DC-link capacitor and voltage are C_{dc} and V_{dc}, respectively. The DER side is designed as a bidirectional power source, which can provide/absorb power to/from the AC side and its power is shown as P_s. The balanced abc frame three-phase PCC voltages and their phase angle are denoted as v_{abc}^{pcc} and θ_g, respectively. Assuming the global dq frame PCC voltages are in the form of $V_d^{pcc} = \sqrt{2}V_{rms}$ and $V_q^{pcc} = 0$, using the reference frame transformation [36] as illustrated in Fig. 2, the local (inverter) dq frame PCC voltages can be expressed as

$$\begin{bmatrix} V_{dl}^{pcc} \\ V_{ql}^{pcc} \end{bmatrix} = \begin{bmatrix} V_d^{pcc}\cos\delta \\ -V_d^{pcc}\sin\delta \end{bmatrix}, \tag{1}$$

where $\delta = \theta - \theta_g$ is the phase angle difference between the DER-sourced inverter and the PCC. Hence, the voltage dynamics of the system in the local inverter dq frame becomes

$$L_f\frac{di_d}{dt} = -R_f i_d + \omega L_f i_q - V_{dl}^{pcc} + V_d \tag{2}$$

$$L_f\frac{di_q}{dt} = -R_f i_q - \omega L_f i_d - V_{ql}^{pcc} + V_q \tag{3}$$

where i_d, i_q and V_d, V_q are the local dq frame inverter currents and voltages, while $\omega = \dot{\theta}$ is the angular frequency of the inverter. Thus, considering (1) and local frame inverter currents, the inverter active and reactive power can be obtained as

$$\begin{aligned} P &= \frac{3}{\sqrt{2}}V_{rms}(i_d\cos\delta - i_q\sin\delta) \\ Q &= -\frac{3}{\sqrt{2}}V_{rms}(i_d\sin\delta + i_q\cos\delta). \end{aligned} \tag{4}$$

It is clear from (4) that the power equations include nonlinear terms. Hence, nonlinear control design and analysis are essential to guarantee a stable behavior of the inverter when power control is required as pointed out in [37], [38]. It is important to mention that since the filter capacitor has very small values in real applications, in this paper, the real and reactive power arriving at the filter capacitor are almost equal to the ones injected to the grid, as mentioned in [39]. Power control is generally implemented via droop control by either coupling $P \sim \omega$ and $Q \sim V$ in high power or inductive output applications or coupling $P \sim V$ and $Q \sim \omega$ in low power or resistive output applications [13], [34]. However, DC-link dynamics are generally ignored by assuming a constant DC voltage in the DER side, which is not realistic in practical applications. To this end, this paper proposes a method, which combines the grid supporting features of the ViSynC approach combined with $Q \sim V$ droop control to introduce virtual inertia and damping, achieve RMS current limitation, and accurate reactive power control, while guaranteeing the closed-loop system stability under balanced grid voltage sags.

III. Proposed Nonlinear Controller, RMS Current Limitation, and ViSynC Integration

A. Proposed Nonlinear Controller and Current Limitation

In this part, the recently proposed sl-PI controller [33] is formulated in a way to achieve both the $Q \sim V$ droop control and the RMS inverter current limitation without using any saturation limits and additional anti-windup techniques. Contrary to the existing approaches [36], which align the local inverter voltage to the d-axis, the proposed control structure is based on the idea of aligning the local inverter current to the d-axis as shown in Fig. 2, i.e. $i_q = 0$, in order to simplify the control implementation and facilitate the closed-loop system stability. To this end, the local dq frame inverter voltages are used as control inputs and formed as

$$V_d = V_{dl}^{pcc} + E_{max}\sin\sigma - r_v i_d - \omega L_f i_q \tag{5}$$

$$V_q = V_{ql}^{pcc} - r_v i_q + \omega L_f i_d \tag{6}$$

where r_v and E_{max} are the main parameters for the sl-PI controller and introduced as virtual resistor and voltage, respectively, to the DER-sourced inverter system. While $\omega L_f i_d$ and $\omega L_f i_q$ represent the dq transformation decoupling terms, σ is the sl-PI controller state and designed as

$$\dot{\sigma} = \frac{c}{E_{max}}\left[(E^* - V_{rms}) - n(Q - Q_{set})\right]\cos\sigma \tag{7}$$

where c is the positive integral gain. As it is proven in [33], if the initial controller state σ_0 is chosen as $\sigma_0 \in [-\frac{\pi}{2}, \frac{\pi}{2}]$, it is ensured that $\sigma(t) \in [-\frac{\pi}{2}, \frac{\pi}{2}], \forall t \geq 0$. Furthermore, since $\dot{\sigma} \to 0$ when $\sigma \to \pm\frac{\pi}{2}$, then the controller inherently provides an integrator anti-windup property by slowing down the

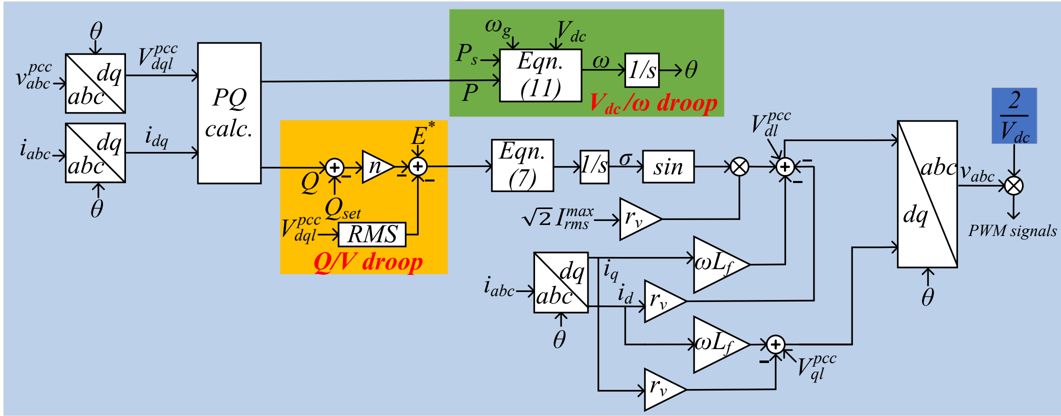

Fig. 3: Implementation diagram of the proposed controller integrated with the ViSynC.

integration near the limits, opposed to conventional saturated integrators.

Note that the $Q \sim V$ droop operation is achieved by regulating the expression $(E^* - V_{rms}) - n(Q - Q_{set})$ to zero using the integrator feature of the sl-PI controller. In this expression, E^*, V_{rms}, n, and Q_{set} denote the rated RMS grid voltage, PCC RMS voltage, reactive power droop coefficient, and reactive power set value, respectively.

Replacing the proposed controller dynamics (5)-(6) in the system dynamics (2)-(3), the closed-loop system current dynamics can be obtained as

$$L_f \frac{di_d}{dt} = -(r_v + R_f)i_d + E_{max}\sin\sigma \tag{8}$$

$$L_f \frac{di_q}{dt} = -(r_v + R_f)i_q \tag{9}$$

The solution of q axis current dynamics (9) can be obtained independently from the closed-loop system dynamics as $i_q(t) = i_q(0)e^{-\frac{(r_v+R_f)}{L_f}t}$, thus if initially $i_q(0) = 0$, then $i_q(t) = 0, \forall t \geq 0$. In order to ensure RMS current limitation and closed-loop stability, the controller parameter can be selected as $E_{max} = (r_v + R_f)I_d^{max}$, where $I_d^{max} = \sqrt{2}I_{rms}^{max}$ and I_{rms}^{max} is the maximum RMS current that the inverter can handle. More precisely, for $\forall t \geq 0$, it holds true that d axis current i_d and the controller state σ remain in the intervals $[-\sqrt{2}I_{rms}^{max}, \sqrt{2}I_{rms}^{max}]$ and $[-\frac{\pi}{2}, \frac{\pi}{2}]$, respectively. Note that the current-limiting property holds for the original nonlinear system and it is also guaranteed independently of the large-signal system faults. The readers can refer to [40] for the current-limiting property and [33] for the controller state limitation, which are realized using nonlinear ultimate boundedness theory.

B. ViSynC Integration

In this part, the ViSynC dynamics, which create an interaction between the DC and AC sides via the $V_{dc} \sim \omega$ droop operation, is combined with the remaining system dynamics (4)-(9) to provide virtual damping and inertia to the system in addition to accurate $Q \sim V$ droop operation and RMS inverter current limitation property, which are ensured via sl-PI controller. To this end, considering $i_q = 0 \ \forall t \geq 0$, as proven in the previous section and replacing it in the power equation (4), the ViSynC dynamics can be obtained as

$$\frac{d}{dt}V_{dc}^2 = \frac{2P_s - 3\sqrt{2}V_{rms}i_d\cos\delta}{C_{dc}} \tag{10}$$

$$\frac{d}{dt}\omega = \frac{2P_s - 3\sqrt{2}V_{rms}i_d\cos\delta}{C_{dc}K_J} + \frac{K_T({V_{dc}}^2 - {V_{dcref}}^2) + K_D(\omega_g - \omega)}{K_J} \tag{11}$$

where P_s is the bidirectional DER power, K_T, K_J, and K_D are DC voltage tracking, inertia, and damping gains, respectively, and ω_g is the rated grid angular frequency. The readers can refer to [16] to explore the SG emulation capability of the ViSynC. The implementation diagram of the proposed controller integrated with the ViSynC is provided in Fig. 3.

IV. Stability Analysis

Although the proposed controller can ensure a desired RMS current-limitation of the inverter based on the sl-PI control structure, the stability of the closed-loop system including the DC link dynamics has not been proven yet. Opposed to conventional approaches that use root locus analysis which investigates the stability of an inverter system for a specific set of parameters, here, singular perturbation theory [35], [38] will be used to obtain analytic stability conditions that can also inform the controller parameter selection (e.g. relationship between virtual inertia and damping values).

A. Closed-Loop System

By considering (7), (8), (10), (11) and $\dot{\delta} = \omega - \omega_g$, and omitting the i_q dynamics (9) from the system since $i_q(t) = 0, \ \forall t \geq 0$, the closed-loop system can be formed as

$$\begin{bmatrix} \dot{i}_d \\ \dot{\sigma} \end{bmatrix} = \begin{bmatrix} L_f^{-1}(r_v + R_f)(-i_d + \sqrt{2}I_{rms}^{max}\sin\sigma) \\ cE_{max}^{-1}\left[(E^* - V_{rms}) - n(Q - Q_{set})\right]\cos\sigma \end{bmatrix} \tag{12}$$

$$\begin{bmatrix} \dot{V}_{dc}^2 \\ \dot{\omega} \\ \dot{\delta} \end{bmatrix} = \begin{bmatrix} C_{dc}^{-1}(2P_s - 3\sqrt{2}V_{rms}i_d\cos\delta) \\ C_{dc}^{-1}K_J^{-1}(2P_s - 3\sqrt{2}V_{rms}i_d\cos\delta \\ +C_{dc}(K_T({V_{dc}}^2 - {V_{dcref}}^2) + K_D(\omega_g - \omega))) \\ \omega - \omega_g \end{bmatrix} \tag{13}$$

For the above system, consider the following assumption.

Assumption 1 (Time-scale separation): The parameters of the equations (7), (8), and (10) should satisfy

$$\max\left\{\frac{L_f}{r_v + R_f}, \frac{1}{c}\right\} \ll C_{dc} \tag{14}$$

Assumption 1 is necessary in order to separate the equations (7) and (8) from the ViSynC dynamics (10), (11), and $\dot{\delta} = \omega - \omega_g$ for a simple closed-loop stability analysis. Note that Assumption 1 can be easily satisfied by choosing the appropriate values for the controller parameters (r_v and c), which can be accomplished by the control operator, compared to the system parameters (L_f and C_{dc}). To ensure the time-scale separation, C_{dc} should have much larger values than $\max\left\{\frac{L_f}{r_v+R_f}, \frac{1}{c}\right\}$, e.g., at least ten times larger as a rule of thumb. As an example, one can check that this condition is satisfied in the system parameters provided in the simulation and HIL implementation cases (Table I).

Consider an equilibrium point $x_e = [i_{de}\ \sigma_e\ V_{dce}^2\ \omega_e\ \delta_e]^T$ obtained from (12)-(13) at the steady state where $\sigma_e \in (-\frac{\pi}{2}, \frac{\pi}{2})$. By setting $\epsilon = \frac{1}{\min\left\{\frac{r_v+R_f}{L_f}, c\right\}}$, there exist $\gamma_a \geq 0$ and $\gamma_b \geq 0$ such that $\frac{r_v+R_f}{L_f} = (1/\epsilon) + \gamma_a$ and $c = (1/\epsilon) + \gamma_b$. Thus, (12) can be rewritten as

$$\begin{bmatrix} \epsilon \dot{i_d} \\ \epsilon \dot{\sigma} \end{bmatrix} = \begin{bmatrix} 1+\epsilon\gamma_a & 0 \\ 0 & 1+\epsilon\gamma_b \end{bmatrix} \begin{bmatrix} (-i_d + \sqrt{2} I_{rms}^{max} \sin\sigma) \\ E_{max}^{-1}\left[(E^* - V_{rms}) - n(Q - Q_{set})\right]\cos\sigma \end{bmatrix}. \tag{15}$$

Thus, the closed-loop system equations (13) and (15) can be written in the form of

$$\dot{x} = f(x, z) \tag{16}$$

$$\epsilon \dot{z} = g(x, z, \epsilon) \tag{17}$$

$$x = \begin{bmatrix} V_{dc}^2 - V_{dce}^2 \\ \omega - \omega_e \\ \delta - \delta_e \end{bmatrix} \qquad z = \begin{bmatrix} i_d - i_{de} \\ \sigma - \sigma_e \end{bmatrix}.$$

For the arbitrarily large values of the virtual resistor r_v and integral gain c, which are the controller parameters, the ϵ value is small and, thus, (16)-(17) can be examined as a singularly perturbed system through the two-time-scale analysis [35]. The system (15) is called as boundary layer, because it represents the immediate vicinity of a bounding surface as mentioned in [35], [41].

B. Boundary Layer Analysis

Considering f, g are continuously differentiable in the domain $(x, z, \epsilon) \in D_x \times D_z \times [0, \epsilon_0]$, when the system and controller parameters are selected according to Assumption 1, then $\epsilon \to 0$ and, based on singular perturbation theory, g will have an algebraic form of $0 = g(x, z)$. The roots of the system can be calculated as

$$\begin{aligned} \bar{i}_d &= \sqrt{2} I_{rms}^{max} \sin\bar{\sigma} \\ \bar{\sigma} &= \sin^{-1}\left(\frac{1}{3V_{rms}\sin\delta I_{rms}^{max}}\left(\frac{V_{rms} - E^*}{n} - Q_{set}\right)\right) \end{aligned} \tag{18}$$

These roots can be assigned as $z = h(x)$ with $\bar{i}_{de} \in [-\sqrt{2} I_{rms}^{max}, \sqrt{2} I_{rms}^{max}]$, and $\bar{\sigma}_e \in (-\frac{\pi}{2}, \frac{\pi}{2})$, such that $h(0) = 0$. Thus, the roots can also be regarded as the equilibrium points of the nonlinear systems (12) and (13). Exponential stability at the origin can be examined using the boundary layer system Jacobian matrix as below

$$J_1 = \begin{bmatrix} -\frac{(r_v+R_f)}{L_f} & \frac{E_{max}\cos\bar{\sigma}}{L_f} \\ \frac{3c}{\sqrt{2}E_{max}} n \cos\bar{\sigma} V_{rms}\sin\delta & 0 \end{bmatrix} \tag{19}$$

The characteristic equation of the system (19)

$$\lambda^2 + \frac{(r_v + R_f)}{L_f}\lambda - \frac{3\sqrt{2} c n \cos^2\bar{\sigma} V_{rms}\sin\delta}{2L_f} = 0 \tag{20}$$

By applying the Routh-Hurwitz criterion, in order for all eigenvalues to have negative real parts, the following two stability conditions are obtained:

$$\sin\delta < 0 \tag{21}$$

$$\bar{\sigma} \in \left(-\frac{\pi}{2}, \frac{\pi}{2}\right) \tag{22}$$

Although (22) can be guaranteed by the proposed controller and the equilibrium point under consideration, condition (21) will be investigated in the sequel.

C. Reduced System Analysis

The reduced model can be found by replacing the roots $\bar{i}_d$ and $\bar{\sigma}$ in (13) as

$$\begin{bmatrix} \dot{V_{dc}^2} \\ \dot{\omega} \\ \dot{\delta} \end{bmatrix} = \begin{bmatrix} C_{dc}^{-1}\left(2P_s - 2\cot\delta\left(\frac{V_{rms}-E^*}{n} - Q_{set}\right)\right) \\ C_{dc}^{-1}K_J^{-1}\left(2P_s - 2\cot\delta\left(\frac{V_{rms}-E^*}{n} - Q_{set}\right) + C_{dc}(K_T({V_{dc}}^2 - {V_{dcref}}^2) + K_D(\omega_g - \omega))\right) \\ \omega - \omega_g \end{bmatrix} \tag{23}$$

The model (23) is usually called as quasi-steady-state model, since $\bar{i}_d$ and $\bar{\sigma}$ introduce a velocity $[\dot{\bar{i}}_d\ \ \dot{\bar{\sigma}}] = \epsilon^{-1} g$ being very large when ϵ is small and $g \neq 0$, inducing a rapid convergence to a root $h(V_{dc}^2, \omega, \delta)$, which is also the equilibrium of the boundary layer system.

Considering (23), the equilibrium point vector of the reduced system $x_e = [V_{dce}^2\ \ \omega_e\ \delta_e]$ can be computed as

$$a)\ V_{dce}^2 = V_{dcref}^2 \tag{24}$$

$$b)\ \ \omega_e = \omega_g \tag{25}$$

$$c)\ \ \delta_e = \cot^{-1}\left(\frac{P_s}{\left(\frac{V_{rms}-E^*}{n} - Q_{set}\right)}\right) \tag{26}$$

To investigate the reduced model closed-loop stability, its Jacobian matrix is given below

$$J_2 = \begin{bmatrix} 0 & 0 & \frac{2}{C_{dc}\sin^2\delta_e}\left(\frac{V_{rms}-E^*}{n} - Q_{set}\right) \\ \frac{K_T}{K_J} & -\frac{K_D}{K_J} & \frac{2}{C_{dc}K_J\sin^2\delta_e}\left(\frac{V_{rms}-E^*}{n} - Q_{set}\right) \\ 0 & 1 & 0 \end{bmatrix}. \tag{27}$$

The characteristic equation of the system (27) can be obtained as

$$\lambda^3 + \frac{K_D}{K_J}\lambda^2 - \frac{2\left(\frac{V_{rms}-E^*}{n} - Q_{set}\right)}{C_{dc}K_J\sin^2\delta_e}\lambda - \frac{2K_T\left(\frac{V_{rms}-E^*}{n} - Q_{set}\right)}{C_{dc}K_J\sin^2\delta_e} = 0 \tag{28}$$

By employing the Routh-Hurwitz criterion, for all system eigenvalues to have negative real parts, the following three stability conditions are obtained:

$$\frac{K_D}{K_J} > 0 \tag{29}$$

$$\left(\frac{V_{rms} - E^*}{n} - Q_{set}\right) < 0 \tag{30}$$

$$K_D > K_J K_T \tag{31}$$

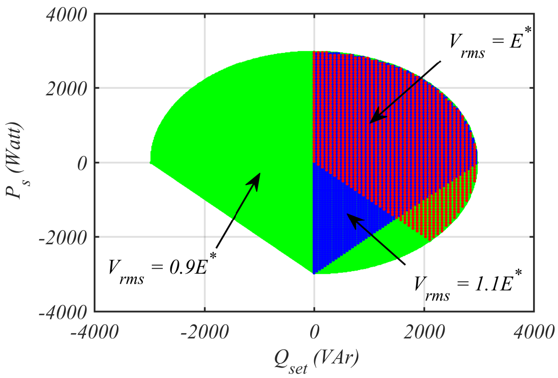

Fig. 4: Regions for selecting P_s and Q_{set} to ensure closed-loop stability.

TABLE I: System and Controller Parameters for Comparison and HIL Studies

Parameters	Values	Parameters	Values
Power System Parameters			
L_f	5.8 mH	L_g	2.2 mH
R_f, R_g	0.5 Ω	V_{dcref}	350 V
ω_g	2π50 rad/s	C_f	1 μF
Simulation		HIL	
S	990 VA	S	2970 VA
E^*	155 V	E^*	110 V
I_{rms}^{max}	3 A	I_{rms}^{max}	9 A
C_{dc}	1000 μF	C_{dc}	2000 μF
Proposed Controller Parameters			
Simulation		HIL	
n	0.0314 V/VAr	n	0.0037 V/VAr
r_v	200 Ω	r_v	30 Ω
c	15000	c	20000
Existing ViSynC Parameters			
k_{pi}, k_{ii}	$0.5, 12$	k_{pv}, k_{iv}	$0.02, 0.2$
K_Q	0.1 V/VAr	V_{qref}	100 V
R_v	0.05 Ω	L_v	0.5 mH
DC-link Controller Parameters			
Simulation		HIL	
K_T	4 Nm/V^2	K_T	4 Nm/V^2
K_J	10 kgm^2	K_J	10 kgm^2
K_D	2500 Nms	K_D	3000 Nms
Comparison HIL Parameters			
RCS		CSA	
k_{pi}, k_{ii}	$10, 50$	k_{pi}, k_{ii}	$10, 50$
k_{pv}, k_{iv}	$10, 100$	k_{pv}, k_{iv}	$10, 100$

Since the gains K_D and K_J are positive, condition (29) always holds. Condition (31) can be guaranteed with the choice of ViSynC gains and it also gives guidance to the users for the appropriate gain selection. Finally, conditions (30) and (21) can be combined considering (26) and following intervals for the power angle can be derived,

$$\pi\,(2n-1) < \delta_e < \tfrac{\pi}{2}\,(4n-1) \quad n \in \mathbb{Z} \tag{32a}$$

$$\tfrac{\pi}{2}\,(4n-1) < \delta_e < 2\pi n \quad n \in \mathbb{Z} \tag{32b}$$

Equation (32a) is valid when the DER power (P_s) is positive, while equation (32b) shows the case when P_s is negative, underlining that stability can be guaranteed for a bidirectional flow of the real power, as required in energy storage devices. Note also that (32a) and (32b) validate condition (21) for the desired equilibrium point, as originally required.

Remark 1: Fig. 4 is plotted considering (26) and gives a guidance on selecting the DER power (P_s) and reactive power set value (Q_{set}) for various values of V_{rms} to guarantee the conditions (21) and (30), using the HIL system parameters provided in Table I.

Therefore, based on the above conditions, the matrices J_1 and J_2 are Hurwitz, and there exist $\eta_1 > 0$ and $\eta_2 > 0$ and domains $\tilde{D}_z = \{z \in \mathbb{R}^2, \|z\|_2 < \eta_1\}$, where $\tilde{D}_z \subseteq D_z$ and $\tilde{D}_x = \{x \in \mathbb{R}^3, \|x\|_2 < \eta_2\}$, where $\tilde{D}_x \subseteq D_x$, such that both the boundary layer model (17) and reduced system (16) are exponentially stable at the origin.

To this end, according to Theorem 11.4 in [35], there exists ϵ^* such that for all $\epsilon < \epsilon^*$, the equilibrium point $x_e = [i_{de}\ \ \sigma_e\ \ V_{dce}^2\ \ \omega_e\ \ \delta_e]^T$ of (16)-(17) with $i_{de} \in [-\sqrt{2}I_{rms}^{max}, \sqrt{2}I_{rms}^{max}]$ and $\sigma_e \in (-\frac{\pi}{2}, \frac{\pi}{2})$ is exponentially stable; thus completing the stability analysis of the entire system.

It should be underlined that since the final stability conditions are found using the Routh-Hurwitz criterion under the worst-case scenarios (i.e., if these conditions hold, then stability is certainly guaranteed), the provided conditions represent the sufficient conditions to guarantee closed-loop system stability and not necessary conditions. Therefore, if the conditions hold, the system will be stable, but if they do not hold, this does not necessarily mean that the system will be certainly led to instability.

V. Comparison with the Commonly Used Methods

In this section, comparison simulation studies based on Matlab/Simulink are realized to justify the theoretical analysis and underline the superior features of the proposed controller scheme compared to existing approaches. In particular, the current-limiting capability and effect of the ViSynC gains on the dynamic system performance are investigated by comparing the proposed method and original method [16], which uses an adaptive current limitation algorithm. The power system and controller parameters are given in Table I. In the following part, the comparison test scenarios are explained in detail.

Scenario I: The simulation starts with 600 W DER input power (P_s) and 400 VAr reactive power reference (Q_{set}). Then, at $t = 4s$, P_s is increased to 800 W, at $t = 8s$, P_s is changed to -500 W to demonstrate the bidirectional active power flow capability of the proposed approach, and at $t = 12s$, P_s is recovered to 600 W. Finally, at $t = 16s$, 40% balanced grid voltage sag is applied and cleared at $t = 17s$. The simulation ends at $t = 20s$. Fig. 5 illustrates this scenario for various values of inertia (K_J) gains. For the original system [16], clamping anti-windup technique is applied in the inner voltage and current PI controllers as mentioned in [20]. The upper (a, b, c, d) subfigures in Fig. 5 show that the original controller [16] can lead to inaccurate reactive power control due to the saturated PI controllers in the inner voltage loop when the DER source demands power, aggressive transients, and current limit violation, while the proposed controller can ensure smooth transients and current limitation at all times as the ViSynC gains are chosen according to the stability conditions. Although increasing K_J can decrease the frequency fluctuation due to higher inertia provision as in Fig. 7, it can have detrimental effects on the original controller performance as presented in the lower subfigures (e, f, g, h) in Fig. 5, while the proposed controller can always guarantee smooth and safe operation.

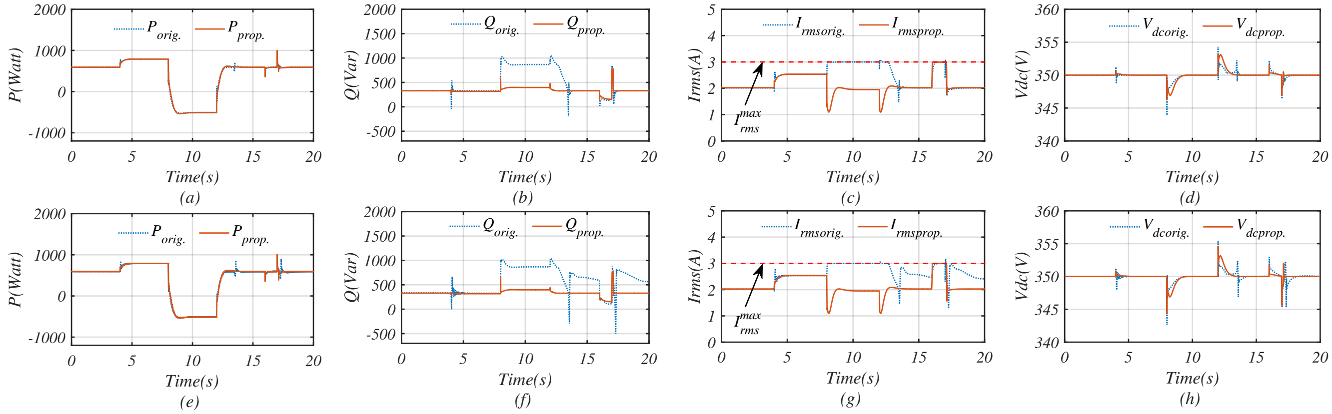

Fig. 5: Performance comparison of the original [16] and the proposed controller. (a), (b), (c), and (d) with $K_J = 10$ kgm^2, (e), (f), (g), and (h) with $K_J = 50$ kgm^2, while $K_T = 4$ Nm/V^2 and $K_D = 2500$ Nms.

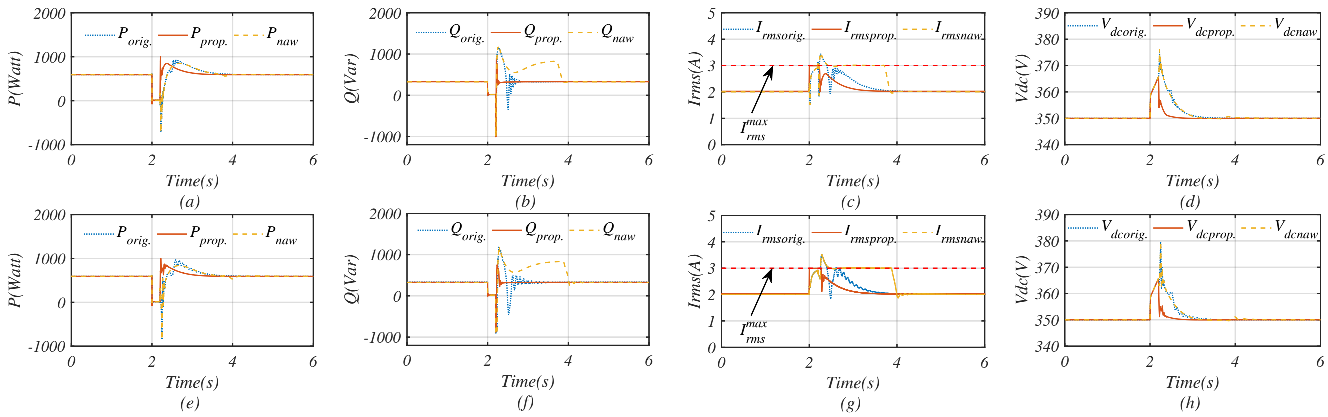

Fig. 6: Performance comparison of the original [16], with (orig.) and without (naw) anti-windup techniques, and the proposed controller in case of a short circuit (a), (b), (c), and (d) with $K_J = 10$ kgm^2, (e), (f), (g), and (h) with $K_J = 50$ kgm^2, while $K_T = 4$ Nm/V^2 and $K_D = 2500$ Nms.

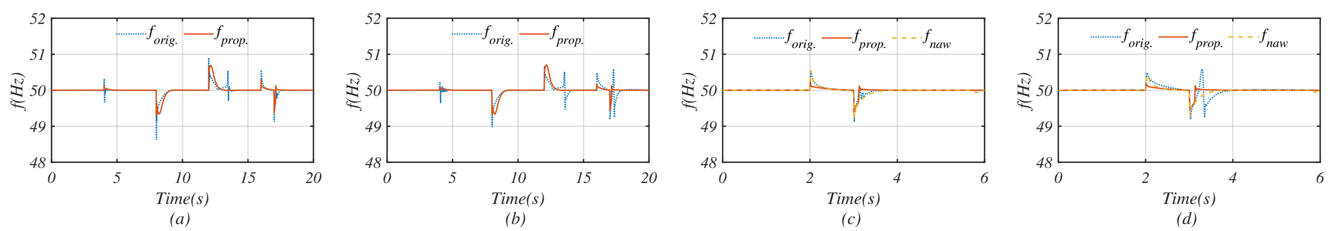

Fig. 7: Frequency comparison of the original [16], with (orig.) and without (naw) anti-windup techniques, and the proposed controller in case of entire scenario (a) with $K_J = 10$ kgm^2 (b) with $K_J = 50$ kgm^2, and in case of a 40% balanced grid fault (c) with $K_J = 10$ kgm^2 (d) with $K_J = 50$ kgm^2, while $K_T = 4$ Nm/V^2 and $K_D = 2500$ Nms

Scenario II: This part focuses on the effect of severe grid voltage sags to the performance of the proposed method and original controller with and without anti-windup techniques when the ViSynC gains vary. The simulation starts with 600 W P_s and 400 VAr Q_{set}. Then, at $t = 2s$, a short circuit grid fault is applied and cleared at $t = 2.2s$. The simulation ends at $t = 6s$. Fig. 6 depicts that the proposed approach shows better performance compared to the original controller, which is either equipped or not-equipped with the anti-windup techniques, by limiting the RMS inverter current at all times and guaranteeing a smooth and fast transient responses. Moreover, Fig. 7 illustrates the frequency damping ability of the proposed approach compared to the original controller. As can be understood from the frequency performances of both the entire case (Scenario I) in Figs. 7 (a) and (b) and 40% balanced voltage sag case in Figs. 7 (c) and (d), the proposed approach leads to lower amplitude frequency oscillations when the inertia gain (K_J) increases. To this end, the superior performance of the proposed method is verified for a number of cases with extensive simulation results compared to the existing methods.

VI. Experimental Studies

In this section, the effectiveness of the proposed method is examined and its advantages compared to the existing state-of-the-art current-limiting methods are demonstrated via hardware-in-the-loop studies.

A. Hardware-In-The-Loop (HIL) Results

In order to verify the dynamic performance of the proposed controller and validate the theoretical stability analysis, a

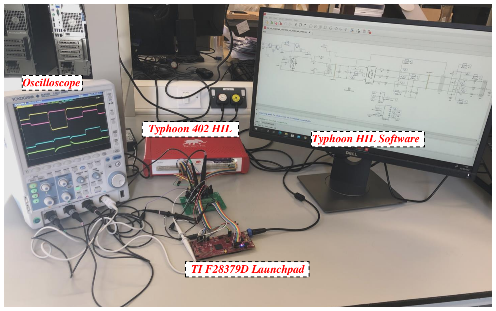

Fig. 8: HIL experimental setup.

DER-sourced three-phase inverter connected to grid is designed using Typhoon-HIL 402 device and the control algorithms, as shown in Fig. 3, are implemented in the TI F28379D launchpad. The experiment setup is provided in Fig. 8. Both the controller sampling and PWM switching frequencies are 20 kHz, while the remained system and controller parameters are provided in Table. I. It should be emphasized here that in a real implementation of the proposed controller, phase-lead low-pass filter can be added to the PCC voltage measurements to overcome small delay and noise issues caused by the inclusion of the feedforward terms in the control algorithm (see [39], [42]).

The following scenario is carried out through HIL implementation. The operation starts with the values of $1200\,\text{W}$ DER input power (P_s) and $1200\,\text{VAr}$ reactive power reference (Q_{set}). At $t = 1s$, P_s is increased to $1800\,\text{W}$, which represents a demand rise in the grid side, at $t = 3s$, P_s is changed to $-1000\,\text{W}$ to test the bidirectional power transfer ability of the proposed method, and at $t = 5s$, P_s is recovered to $1800\,\text{W}$. In order to verify the integrator windup-free operation and current-limiting property under a considerable system fault, at $t = 7s$, a 40% balanced grid voltage sag is applied, and at $t = 9s$, the fault is cleared. The operation ends at $t = 10s$. Note that since the $Q \sim V$ droop is always enabled during the operation, reactive power is not regulated to exact Q_{set} values to support the grid voltage.

As can be seen in Figs. 9 and 10, the proposed control scheme can rapidly regulate both the active and reactive power and limit the inverter RMS current without any controller saturation even after a grid voltage sag. In order to guide the prospective users about the ViSynC gain selections, Fig. 9 illustrates the effect of various damping gain (K_D) values on the system behavior, while Fig. 10 demonstrates the influence of inertia (K_J) and DC voltage tracking (K_T) gains on the dynamic system performance. The results are taken by considering constant $K_J = 10$ kgm^2 and $K_T = 4$ Nm/V^2 and variable K_D in Fig. 9. Although increasing K_D can decrease the steady state system oscillations as shown in Fig. 9a and 9b, it increases DC voltage (V_{dc}) fluctuation when the DER source demands power as in Fig. 9c. Therefore, K_D is chosen as 3000 Nms while taking the results in Fig. 10. Choosing large K_J values can cause surges in oscillation magnitudes as shown in Fig. 10a and 10b, while selecting large K_T gain can lead to faster dynamic response. The transient performance of the proposed current-limiting method is illustrated through

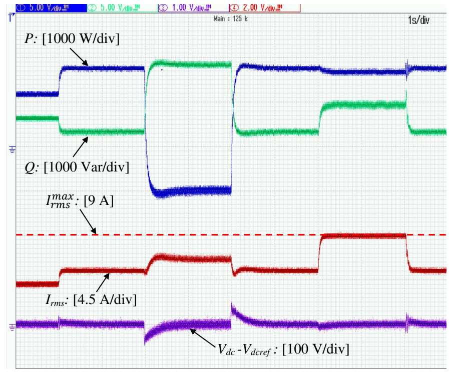

(a) Time response of P, Q, I_{rms} and V_{dc} when K_D = 2000 Nms

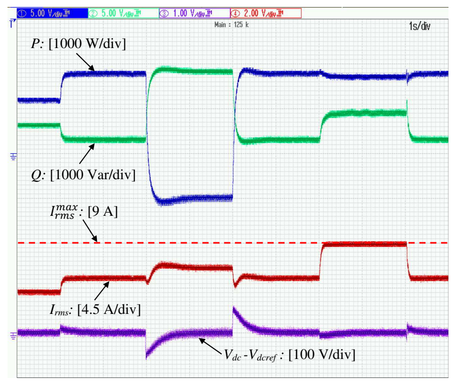

(b) Time response of P, Q, I_{rms} and V_{dc} when K_D = 3000 Nms

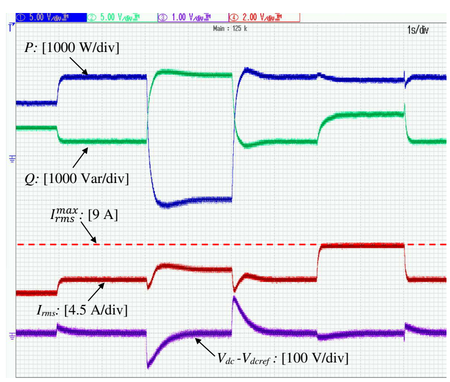

(c) Time response of P, Q, I_{rms} and V_{dc} when K_D = 5000 Nms

Fig. 9: HIL results of a DER-sourced inverter under the proposed controller with different K_D gains.

instantaneous inverter current and PCC voltage waveforms in Fig. 11 when $P_s = 1800\,\text{W}$. While Fig. 11a shows that the inverter currents are limited during the grid fault appearance, Fig. 11b also demonstrates that there is no current limit violation during the grid fault recovery. It is important to note that due to the four available channels in the oscilloscope, one phase PCC voltage (v_a) and three-phase inverter currents (i_a, i_b, i_c) are shown in Fig. 11. However, since the balanced grid fault is applied, the other voltage phases follow the same voltage drop as phase a. In order to test the proposed controller performance under grid frequency (ω_g) changes, by selecting

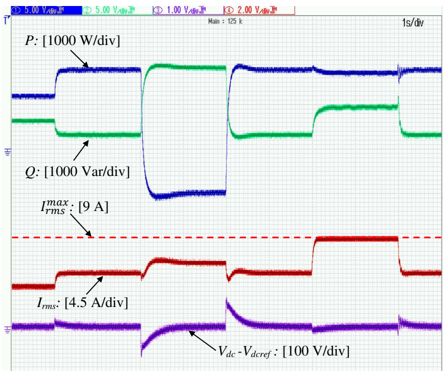

(a) Time response of P, Q, I_{rms} and V_{dc} when K_T = 4 Nm/V^2 and K_J = 20 kgm^2

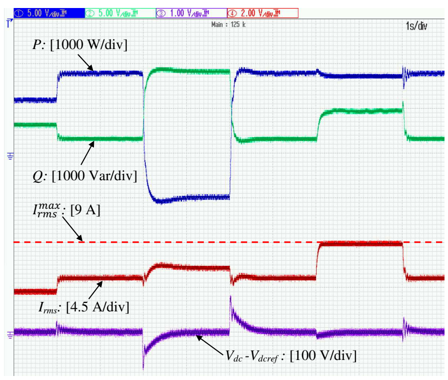

(b) Time response of P, Q, I_{rms} and V_{dc} when K_T = 4 Nm/V^2 and K_J = 50 kgm^2

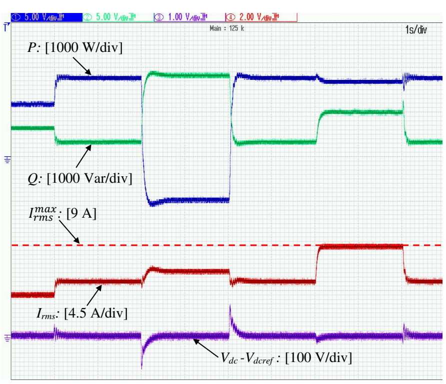

(c) Time response of P, Q, I_{rms} and V_{dc} when K_T = 10 Nm/V^2 and K_J = 30 kgm^2

Fig. 10: HIL results of a DER-sourced inverter under the proposed controller with different K_J and K_T gains.

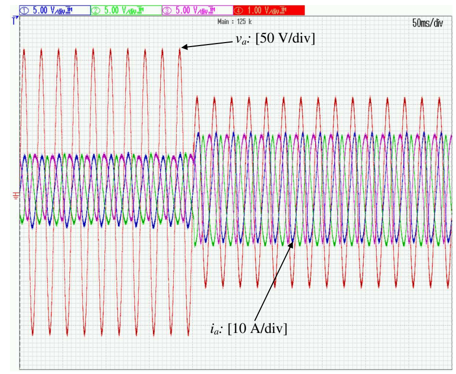

(a) Three-phase instantaneous inverter currents (i_{abc}) and PCC voltage (v_a) waveforms when the grid fault occurs

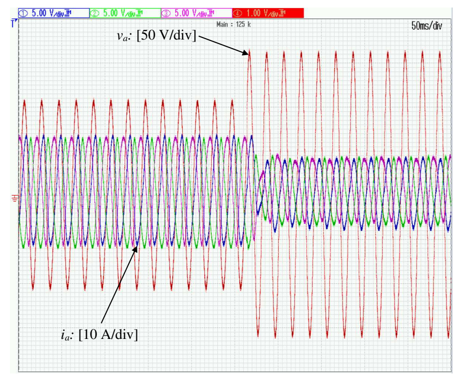

(b) Three-phase instantaneous inverter currents (i_{abc}) and PCC voltage (v_a) waveforms when the grid fault is cleared

Fig. 11: HIL results of a DER-sourced inverter under the proposed controller in case of a balanced voltage sag (a) 110 V $\rightarrow$ 70 V and recovery (b) 70 V $\rightarrow$ 110 V

K_T = 4 Nm/V^2, K_J = 10 kgm^2, K_D = 3000 Nms, and the frequency weighting coefficient $m = 0.1$ as explained in [16], an other HIL scenario is realized in Fig. 12. By keeping the other changes same with the previous results, at $t = 7s$, the grid frequency is decreased to 49 Hz in Fig. 12a and increased to 51 Hz in Fig. 12b, and at $t = 9s$, the grid frequency comes back to its nominal value. Thus, it is proven that the proposed controller maintains the system stability and provides virtual inertia via $V_{dc} \sim \omega$ coupling as proven in Section IV. Furthermore, the boundary of ViSynC gain selection is verified to prove the validity of stability condition (31) in Fig. 13. Fig. 13a shows that the system becomes oscillatory in both transients and steady-state when the gains are chosen close to the stability boundary, while Fig. 13b demonstrates that the system loses its stability if the gains violate inequality (31). However, in both oscillatory and unstable cases, the proposed method limits the inverter current without the need of algorithm change and saturation blocks as seen in Fig. 13. As a result, it is verified that the proposed approach can limit the RMS inverter current without any dependence on the ViSynC gains, and the selection of the ViSynC gains K_J, K_D and K_T in order to satisfy the stability condition (31) further supports the theoretic analysis presented in this work.

B. Comparison Studies via Hardware-In-The-Loop Results

In this section, the superior features of the proposed method are emphasized by comparing it with two state-of-the-art current-limiting algorithms. The methods, which are used for comparison, are reference current saturation (RCS) [36] and d-axis priority based-current saturation algorithm (CSA) [43]. The system and controller parameters are provided in Table I. The same system scenario with the Section VI-A is implemented in this part. Even though the proposed method is stable for smaller damping gain (K_D), since the comparison methods need very high damping gain for stability, a larger damping gain (K_D = 30000 Nms) is used while taking the

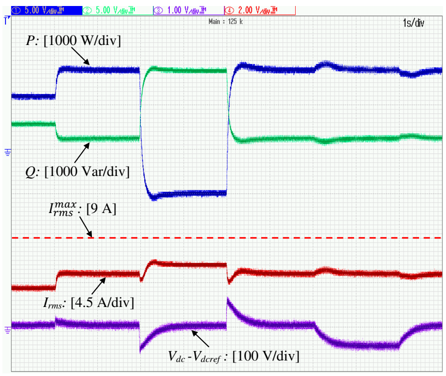

(a) Time response of P, Q, I_{rms} and V_{dc} in case of grid frequency drop

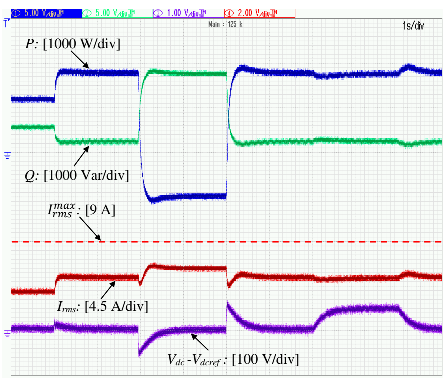

(b) Time response of P, Q, I_{rms} and V_{dc} in case of grid frequency swell

Fig. 12: HIL results of a DER-sourced inverter under the proposed controller when the grid frequency (ω_g) changes.

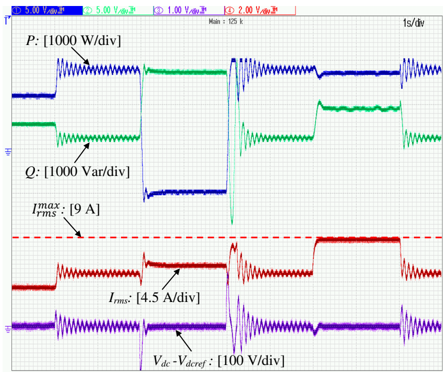

(a) Time response of P, Q, I_{rms} and V_{dc} when $K_D = 3000$ Nms, $K_J = 200$ kgm^2, and $K_T = 10$ Nm/V^2

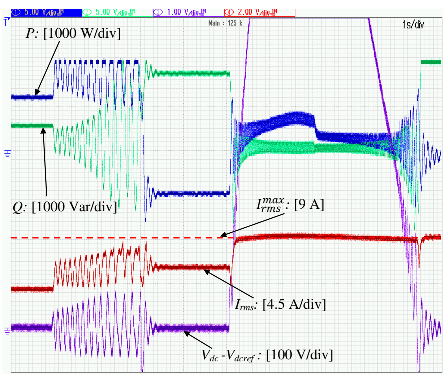

(b) Time response of P, Q, I_{rms} and V_{dc} when $K_D = 3000$ Nms, $K_J = 200$ kgm^2, and $K_T = 20$ Nm/V^2

Fig. 13: HIL results of a DER-sourced inverter under the proposed controller when the stability condition (31) is tested.

results for all three controllers. As shown in Fig. 14, although all three methods maintain the stable operation of the system, only the proposed method can always guarantee the desired current-limiting property and damped system response, as shown in Fig. 14a. Both the d-axis priority based-CSA and RCS violate the current limit (9 A), when the grid fault occurs and is cleared as can be seen in Figs. 14b and 14c, respectively. Besides, when the P_s value is changed from positive to negative and from negative to positive, d-axis priority based-CSA method leads to an oscillatory response as illustrated in Fig. 14b. Thus, it is verified that the proposed method can guarantee the current limitation and closed-loop system stability, when the gains are selected to satisfy (31), while the other methods fail to provide those properties throughout the entire operation.

VII. Conclusion

A nonlinear current-limiting controller, which combines the ViSynC and droop control dynamics, has been proposed in this paper for a three-phase inverter-integrated DER unit. The RMS current-limiting property was ensured throughout the operation, even under severe balanced voltage sags, independently from the controller and ViSynC parameters without the need of an algorithm change or saturation units. The closed-loop system stability has been rigorously proven using the singular perturbation theory, while analytic stability conditions, which guide the users for controller gain and reference power selections to guarantee the closed-loop stability, were provided. The proposed method has been compared with the state-of-the-art current-limiting methods and its superior features have been highlighted with extensive simulation studies. The stability conditions and dynamic performance of the proposed controller were also verified via comprehensive HIL results and compared to the existing techniques.

Acknowledgment

The authors would like to thank Typhoon HIL Inc. that supported the validation process of this research with their donation of HIL-402 device.

References

[1] A. Tayyebi, D. Groß, A. Anta, F. Kupzog and F. Dörfler, “Frequency Stability of Synchronous Machines and Grid-Forming Power Converters,” *IEEE Journal of Emerging and Selected Topics in Power Electronics*, vol. 8, no. 2, pp. 1004-1018, June 2020, doi: 10.1109/JESTPE.2020.2966524.

[2] T. Dragicevic, S. Vazquez and P. Wheeler, "Advanced Control Methods for Power Converters in DG Systems and Microgrids," *IEEE Transactions on Industrial Electronics*, doi: 10.1109/TIE.2020.2994857.

[3] K. S. Ratnam, K. Palanisamy, and G. Yang, “Future low-inertia power systems: Requirements, issues, and solutions - A review,” *Renewable and Sustainable Energy Reviews*, vol. 124, no. February, 2020, doi: 10.1016/j.rser.2020.109773.

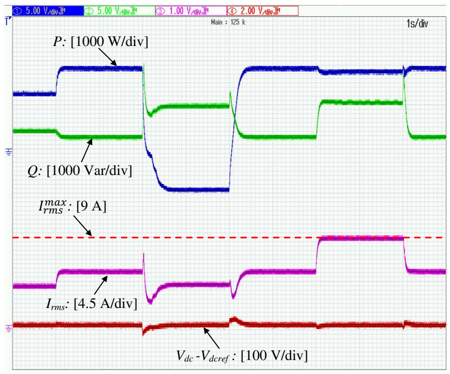

(a) Time response of P, Q, I_{rms} and V_{dc} when the proposed controller is used

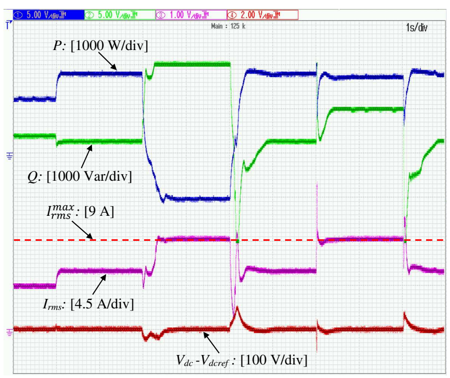

(b) Time response of P, Q, I_{rms} and V_{dc} when the d-axis priority based-current saturation algorithm in [43] is used

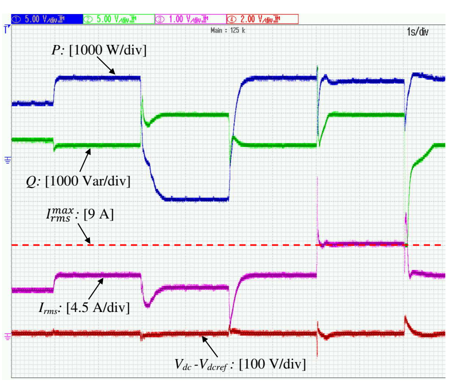

(c) Time response of P, Q, I_{rms} and V_{dc} when the reference current saturation method in [36] is used

Fig. 14: HIL comparison results of a DER-sourced inverter under proposed and conventional current-limiting methods ([36] and [43]) when $K_D = 30000$ Nms, $K_J = 10$ kgm^2, and $K_T = 10$ Nm/V^2.

[4] X. Hou, Y. Sun, X. Zhang, J. Lu, P. Wang and J. M. Guerrero, “Improvement of Frequency Regulation in VSG-Based AC Microgrid Via Adaptive Virtual Inertia," *IEEE Transactions on Power Electronics*, vol. 35, no. 2, pp. 1589-1602, Feb. 2020, doi: 10.1109/TPEL.2019.2923734.

[5] J. Liu, Y. Miura, H. Bevrani and T. Ise, “Enhanced Virtual Synchronous Generator Control for Parallel Inverters in Microgrids," *IEEE Transactions on Smart Grid*, vol. 8, no. 5, pp. 2268-2277, Sept. 2017, doi: 10.1109/TSG.2016.2521405.

[6] M. G. Taul, X. Wang, P. Davari and F. Blaabjerg, “An Overview of Assessment Methods for Synchronization Stability of Grid-Connected Converters Under Severe Symmetrical Grid Faults," *IEEE Transactions on Power Electronics*, vol. 34, no. 10, pp. 9655-9670, Oct. 2019, doi: 10.1109/TPEL.2019.2892142.

[7] J. Fang, H. Li, Y. Tang and F. Blaabjerg, “Distributed Power System Virtual Inertia Implemented by Grid-Connected Power Converters," *IEEE Transactions on Power Electronics*, vol. 33, no. 10, pp. 8488-8499, Oct. 2018, doi: 10.1109/TPEL.2017.2785218.

[8] P. Mancarella and F. Billimoria, “The Fragile Grid: The Physics and Economics of Security Services in Low-Carbon Power Systems," *IEEE Power and Energy Magazine*, vol. 19, no. 2, pp. 79-88, March-April 2021, doi: 10.1109/MPE.2020.3043570.

[9] J. Liu, Y. Miura and T. Ise, “Comparison of Dynamic Characteristics Between Virtual Synchronous Generator and Droop Control in Inverter-Based Distributed Generators," *IEEE Transactions on Power Electronics*, vol. 31, no. 5, pp. 3600-3611, May 2016, doi: 10.1109/TPEL.2015.2465852.

[10] F. Dörfler, S. Bolognani, J. W. Simpson-Porco and S. Grammatico, “Distributed Control and Optimization for Autonomous Power Grids," *2019 18th European Control Conference (ECC)*, Naples, Italy, 2019, pp. 2436-2453, doi: 10.23919/ECC.2019.8795974.

[11] J. Fang, P. Lin, H. Li, Y. Yang and Y. Tang, “An Improved Virtual Inertia Control for Three-Phase Voltage Source Converters Connected to a Weak Grid," *IEEE Transactions on Power Electronics*, vol. 34, no. 9, pp. 8660-8670, Sept. 2019, doi: 10.1109/TPEL.2018.2885513.

[12] A. F. Hoke, M. Shirazi, S. Chakraborty, E. Muljadi and D. Maksimovic, “Rapid Active Power Control of Photovoltaic Systems for Grid Frequency Support," *IEEE Journal of Emerging and Selected Topics in Power Electronics*, vol. 5, no. 3, pp. 1154-1163, Sept. 2017, doi: 10.1109/JESTPE.2017.2669299.

[13] U. B. Tayab, M. A. Bin Roslan, L. J. Hwai, and M. Kashif, “A review of droop control techniques for microgrid,” *Renewable and Sustainable Energy Reviews*, vol. 76, no. November 2016, pp. 717–727, 2017, doi: 10.1016/j.rser.2017.03.028.

[14] D. Pan, X. Wang, F. Liu and R. Shi, “Transient Stability of Voltage-Source Converters With Grid-Forming Control: A Design-Oriented Study," *IEEE Journal of Emerging and Selected Topics in Power Electronics*, vol. 8, no. 2, pp. 1019-1033, June 2020, doi: 10.1109/JESTPE.2019.2946310.

[15] C. Arghir and F. Dörfler, “The Electronic Realization of Synchronous Machines: Model Matching, Angle Tracking, and Energy Shaping Techniques," *IEEE Transactions on Power Electronics*, vol. 35, no. 4, pp. 4398-4410, April 2020, doi: 10.1109/TPEL.2019.2939710.

[16] L. Huang et al., “A Virtual Synchronous Control for Voltage-Source Converters Utilizing Dynamics of DC-Link Capacitor to Realize Self-Synchronization," *IEEE Journal of Emerging and Selected Topics in Power Electronics*, vol. 5, no. 4, pp. 1565-1577, Dec. 2017, doi: 10.1109/JESTPE.2017.2740424.

[17] D. Pan, X. Wang, F. Liu and R. Shi, “Transient Stability of Voltage-Source Converters With Grid-Forming Control: A Design-Oriented Study," *IEEE Journal of Emerging and Selected Topics in Power Electronics*, vol. 8, no. 2, pp. 1019-1033, June 2020, doi: 10.1109/JESTPE.2019.2946310.

[18] Z. Shuai, C. Shen, X. Liu, Z. Li and Z. J. Shen, “Transient Angle Stability of Virtual Synchronous Generators Using Lyapunov’s Direct Method," *IEEE Transactions on Smart Grid*, vol. 10, no. 4, pp. 4648-4661, July 2019, doi: 10.1109/TSG.2018.2866122.

[19] M. G. Taul, X. Wang, P. Davari and F. Blaabjerg, “Current Limiting Control With Enhanced Dynamics of Grid-Forming Converters During Fault Conditions," *IEEE Journal of Emerging and Selected Topics in Power Electronics*, vol. 8, no. 2, pp. 1062-1073, June 2020, doi: 10.1109/JESTPE.2019.2931477.

[20] L. Huang, H. Xin, Z. Wang, L. Zhang, K. Wu and J. Hu, “Transient Stability Analysis and Control Design of Droop-Controlled Voltage Source Converters Considering Current Limitation," *IEEE Transactions on Smart Grid*, vol. 10, no. 1, pp. 578-591, Jan. 2019, doi: 10.1109/TSG.2017.2749259.

[21] A. D. Paquette and D. M. Divan, “Virtual Impedance Current Limiting for Inverters in Microgrids With Synchronous Generators," *IEEE Transactions on Industry Applications*, vol. 51, no. 2, pp. 1630-1638, March-April 2015, doi: 10.1109/TIA.2014.2345877.

[22] J. M. Guerrero, J. Matas, L. Garcia de Vicuna, M. Castilla and J. Miret, “Decentralized Control for Parallel Operation of Distributed Generation Inverters Using Resistive Output Impedance," *IEEE Transactions on Industrial Electronics*, vol. 54, no. 2, pp. 994-1004, April 2007, doi: 10.1109/TIE.2007.892621.

[23] J. He and Y. W. Li, “Analysis, Design, and Implementation of Virtual Impedance for Power Electronics Interfaced Distributed Generation,"

IEEE Transactions on Industry Applications, vol. 47, no. 6, pp. 2525-2538, Nov.-Dec. 2011, doi: 10.1109/TIA.2011.2168592.

[24] T. Qoria, F. Gruson, F. Colas, G. Denis, T. Prevost and X. Guillaud, “Critical Clearing Time Determination and Enhancement of Grid-Forming Converters Embedding Virtual Impedance as Current Limitation Algorithm," *IEEE Journal of Emerging and Selected Topics in Power Electronics*, vol. 8, no. 2, pp. 1050-1061, June 2020, doi: 10.1109/JESTPE.2019.2959085.

[25] S. Yazdani, M. Ferdowsi, M. Davari and P. Shamsi, “Advanced Current-Limiting and Power-Sharing Control in a PV-Based Grid-Forming Inverter Under Unbalanced Grid Conditions," *IEEE Journal of Emerging and Selected Topics in Power Electronics*, vol. 8, no. 2, pp. 1084-1096, June 2020, doi: 10.1109/JESTPE.2019.2959006.

[26] L. Zhou et al., “Harmonic Current and Inrush Fault Current Coordinated Suppression Method for VSG Under Non-ideal Grid Condition," *IEEE Transactions on Power Electronics*, vol. 36, no. 1, pp. 1030-1042, Jan. 2021, doi: 10.1109/TPEL.2020.3000522.

[27] Z. Shuai, W. Huang, C. Shen, J. Ge and Z. J. Shen, “Characteristics and Restraining Method of Fast Transient Inrush Fault Currents in Synchronverters," *IEEE Transactions on Industrial Electronics*, vol. 64, no. 9, pp. 7487-7497, Sept. 2017, doi: 10.1109/TIE.2017.2652362.

[28] J. Jongudomkarn, J. Liu and T. Ise, “Virtual Synchronous Generator Control With Reliable Fault Ride-Through Ability: A Solution Based on Finite-Set Model Predictive Control," *IEEE Journal of Emerging and Selected Topics in Power Electronics*, vol. 8, no. 4, pp. 3811-3824, Dec. 2020, doi: 10.1109/JESTPE.2019.2942943.

[29] N. Bottrell and T. C. Green, “Comparison of Current-Limiting Strategies During Fault Ride-Through of Inverters to Prevent Latch-Up and Wind-Up," *IEEE Transactions on Power Electronics*, vol. 29, no. 7, pp. 3786-3797, July 2014, doi: 10.1109/TPEL.2013.2279162.

[30] G. C. Konstantopoulos, Q. -. Zhong, B. Ren and M. Krstic, “Bounded Integral Control of Input-to-State Practically Stable Nonlinear Systems to Guarantee Closed-Loop Stability," *IEEE Transactions on Automatic Control*, vol. 61, no. 12, pp. 4196-4202, Dec. 2016, doi: 10.1109/TAC.2016.2552978.

[31] Q. Zhong, G. C. Konstantopoulos, B. Ren and M. Krstic, “Improved Synchronverters with Bounded Frequency and Voltage for Smart Grid Integration," *IEEE Transactions on Smart Grid*, vol. 9, no. 2, pp. 786-796, March 2018, doi: 10.1109/TSG.2016.2565663.

[32] Q. Zhong and G. C. Konstantopoulos, “Current-Limiting Three-Phase Rectifiers," *IEEE Transactions on Industrial Electronics*, vol. 65, no. 2, pp. 957-967, Feb. 2018, doi: 10.1109/TIE.2017.2696483.

[33] G. C. Konstantopoulos and P. R. Baldivieso-Monasterios, “State-limiting PID controller for a class of nonlinear systems with constant uncertainties,” *International Journal of Robust and Nonlinear Control*, vol. 30, no. 5, pp. 1770-1787, 2020, doi: 10.1002/rnc.4853.

[34] S. Dedeoglu, G. C. Konstantopoulos and A. G. Paspatis, “Grid-Supporting Three-Phase Inverters with Inherent RMS Current Limitation Under Balanced Grid Voltage Sags," *IEEE Transactions on Industrial Electronics*, doi: 10.1109/TIE.2020.3034860.

[35] H. K. Khalil, *Nonlinear Systems*, 3rd ed. London, U.K.: Pearson, 2014.

[36] N. Pogaku, M. Prodanovic and T. C. Green, “Modeling, Analysis and Testing of Autonomous Operation of an Inverter-Based Microgrid," *IEEE Transactions on Power Electronics*, vol. 22, no. 2, pp. 613-625, March 2007, doi: 10.1109/TPEL.2006.890003.

[37] I. Sefa, S. Ozdemir, H. Komurcugil and N. Altin, “An Enhanced Lyapunov-Function Based Control Scheme for Three-Phase Grid-Tied VSI With LCL Filter," *IEEE Transactions on Sustainable Energy*, vol. 10, no. 2, pp. 504-513, April 2019, doi: 10.1109/TSTE.2018.2833809.

[38] M. Kabalan, P. Singh and D. Niebur, “Nonlinear Lyapunov Stability Analysis of Seven Models of a DC/AC Droop Controlled Inverter Connected to an Infinite Bus," *IEEE Transactions on Smart Grid*, vol. 10, no. 1, pp. 772-781, Jan. 2019, doi: 10.1109/TSG.2017.2752146.

[39] Q. -C. Zhong and G. C. Konstantopoulos, “Current-Limiting Droop Control of Grid-Connected Inverters," *IEEE Transactions on Industrial Electronics*, vol. 64, no. 7, pp. 5963-5973, July 2017, doi: 10.1109/TIE.2016.2622402.

[40] S. Dedeoglu and G. C. Konstantopoulos, “PLL-Less Three-Phase Droop-Controlled Inverter with Inherent Current-Limiting Property," *IECON 2019 - 45th Annual Conference of the IEEE Industrial Electronics Society*, Lisbon, Portugal, 2019, pp. 4013-4018, doi: 10.1109/IECON.2019.8927219.

[41] A.-C. Braitor, G. C. Konstantopoulos and V. Kadirkamanathan, “Current-Limiting Droop Control Design and Stability Analysis for Paralleled Boost Converters in DC Microgrids," *IEEE Transactions on Control Systems Technology*, vol. 29, no. 1, pp. 385-394, Jan. 2021, doi: 10.1109/TCST.2019.2951092.

[42] Q.-C. Zhong and T. Hornik, *Control of Power Inverters in Renewable Energy and Smart Grid Integration*. Hoboken, NJ, USA: Wiley, 2013.

[43] T. Qoria, F. Gruson, F. Colas, X. Kestelyn, and X. Guillaud, “Current limiting algorithms and transient stability analysis of grid-forming VSCs," *Electric Power System Research*, vol. 189, no. 691800, 2020, doi: 10.1016/j.epsr.2020.106726.

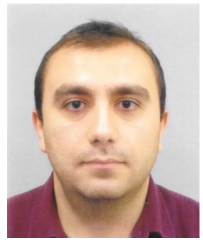

Seyfullah Dedeoglu (Student Member, IEEE) received his Diploma degree from the Department of Electrical and Electronics Engineering, Sakarya University, Sakarya, Turkey, in 2014, and Master degree from the Department of Automatic Control and Systems Engineering, The University of Sheffield, Sheffield, UK, in 2017, where he is currently working towards the Ph.D. degree. In 2015, he got a scholarship that fully covers his Master and PhD education from the Ministry of National Education of Turkey. His current research interests include nonlinear control and stability analysis of unidirectional and bidirectional power converters in renewable energy and smart grid applications.

George C. Konstantopoulos (Member, IEEE) received his Dipl.Eng. and Ph.D. degrees in electrical and computer engineering from the Department of Electrical and Computer Engineering, University of Patras, Rion, Greece, in 2008 and 2012, respectively. From 2011 to 2012, he was an Electrical Engineer with the Public Power Corporation of Greece. Since 2013, he has been with the Department of Automatic Control and Systems Engineering, The University of Sheffield, U.K., holding the positions of Research Associate, Research Fellow, Lecturer and Senior Lecturer. Since 2019, he has been with the Department of Electrical and Computer Engineering, University of Patras, Greece, as an Associate Professor. He is an EPSRC UKRI Innovation Fellow in the priority area of cheap and clean energy technologies and he currently serves as an Associate Editor of the IET Smart Grid Journal and the International Journal of Systems Science. His research interests include nonlinear modeling, control and stability analysis of power converters in microgrid and smart grid applications, renewable energy systems and electrical drives. Dr. Konstantopoulos is a Member of the National Technical Chamber of Greece.

Hasan Komurcugil (Senior Member, IEEE) received the B.Sc., M.Sc. and Ph.D. degrees from the Eastern Mediterranean University (EMU), Famagusta, North Cyprus, Via Mersin 10, Turkey, in 1989, 1991, and 1998, respectively, all in electrical engineering. From 2004 to 2010, he was the Head of the Computer Engineering Department, EMU. In 2010, he was elected as the as the Board Member of Higher Education, Planning, Evaluation, Accreditation and Coordination Council (YODAK) North Cyprus. He is currently full-time Professor with the Computer Engineering Department, EMU. His research interests include power electronics and innovative control methods for power converters such as sliding mode control, Lyapunov-based control, and model predictive control. He is a coauthor of one book (Multilevel Inverters: Introduction and Emergent Topologies) chapter. He is a member of the IEEE Industrial Electronics Society and Senior Member of the IEEE. Also, he is the Chair of the Renewable Energy Systems Subcommitee of Power Electronics Technical Committee of IES. He served as the Corresponding Guest Associate Editor of the IEEE TRANSACTIONS ON ENERGY CONVERSION and Guest Editor of the IEEE TRANSACTIONS ON INDUSTRIAL INFORMATICS. Currently, he serves as the Associate Editor of the IEEE TRANSACTIONS ON INDUSTRIAL ELECTRONICS and the IEEE TRANSACTIONS ON INDUSTRIAL INFORMATICS.